Published for SISSA by Springer

Received: November 26, 2014
Accepted: January 31, 2015
Published: February 25, 2015

Light-by-light scattering with intact protons at the LHC: from standard model to new physics

Sylvain Fichet,[a] **Gero von Gersdorff,**[b] **Bruno Lenzi,**[c] **Christophe Royon**[d] **and Matthias Saimpert**[d]

[a] *International Institute of Physics, UFRN, Av. Odilon Gomes de Lima, 1722 Natal-RN, Brazil*
[b] *ICTP South American Institute for Fundamental Research, Instituto de Fisica Teorica, Sao Paulo State University, Brazil*
[c] *CERN, CH-1211 Geneva 23, Switzerland*
[d] *IRFU/Service de Physique des Particules, CEA/Saclay, 91191 Gif-sur-Yvette cedex, France*

E-mail: sylvain.fichet@lpsc.in2p3.fr, gersdorff@gmail.com, bruno.lenzi@cern.ch, christophe.royon@cea.fr, matthias.saimpert@cern.ch

Abstract: We discuss the discovery potential of light-by-light scattering at the Large Hadron Collider (LHC), induced by the Standard Model (SM) and by new exotic charged particles. Our simulation relies on intact proton detection in the planned forward detectors of CMS and ATLAS. The full four-photon amplitudes generated by any electrically charged particles of spins 1/2 and 1, including the SM processes involving loops of leptons, quarks and W bosons are implemented in the Forward Physics Monte Carlo generator. Our method provides model-independent bounds on massive charged particles, only parametrized by the spin, mass and "effective charge" $Q_{\rm eff}$ of the new particle. We find that a new charged vector (fermion) with $Q_{\rm eff} = 4$ can be discovered up to $m = 700\,\text{GeV}$ ($m = 370\,\text{GeV}$) with an integrated luminosity of $300\,\text{fb}^{-1}$ at the LHC. We also discuss the sensitivities to neutral particles such as a strongly-interacting heavy dilaton and warped Kaluza-Klein gravitons, whose effects could be discovered for masses in the multi-TeV range.

Keywords: Phenomenology of Large extra dimensions

ArXiv ePrint: 1411.6629

doi:10.1007/JHEP02(2015)165

JHEP02(2015)165

Contents

1 Introduction **2**

2 Standard Model exclusive di-photon production **3**
- 2.1 Equivalent Photon Approximation 3
- 2.2 Standard Model exclusive di-photon production 4

3 Effects of new charged particles on exclusive di-photon production **5**
- 3.1 General considerations 5
- 3.2 Effective Field Theory (EFT) 7
- 3.3 Exact amplitudes 9

4 The forward proton detectors **9**

5 Setup of the simulation **10**
- 5.1 Event generation with the Forward Physics Monte Carlo Generator 10
- 5.2 Background simulation and event reconstruction 11

6 Event selection **12**

7 Expected sensitivity for charged particles at the 14 TeV LHC **13**
- 7.1 EFT results 14
- 7.2 Results from exact amplitudes 15
- 7.3 Comparison with the muon $g-2$ measurement 16

8 Neutral contributions to light-by-light scattering **17**

9 Conclusion **20**

A The full one-loop amplitudes **21**
- A.1 Loop functions 21
- A.2 Amplitudes 22

B Limits **23**
- B.1 Low-energy approximation 23
- B.2 High-energy approximation 23
- B.3 Forward and backward limits 23

C Expressions for the amplitudes in EFT **24**

JHEP02(2015)165

1 Introduction

A strong theoretical prejudice exists that New Physics (NP) beyond the Standard Model (SM) should appear around the TeV scale. However, after the first LHC run, a certain amount of popular models has been ruled out or they are cornered in fine-tuned regions of their parameter space. While the next LHC run is coming, it is more than ever important to be prepared to search for any kind of NP in the most possible robust ways.

A lot of models of physics beyond the SM predict the existence of new heavy particles with exotic electric charges. This happens for example in composite Higgs models, which require the existence of new charged particles of spin $\frac{1}{2}$ and 1. In particular, the large mass of the top quark requires the existence of a composite top partner mixing with the elementary one. As the composite sector typically possesses a large global symmetry group, these top partners are accompanied by other resonances with exotic electric charges such as $\frac{5}{3}$ and $\frac{8}{3}$ [1]. New particles with exotic electric charges can also appear in warped extra-dimension models with custodial symmetry [2].

Certain types of these particles are already constrained by direct searches at the LHC. Such direct searches are powerful in specific cases, but are highly model-dependent. Indeed, the production cross sections, decay chains and branching ratios all depend in general on the details of the model. Therefore a specific analysis has to be tailored in each case, as both the final states and the backgrounds are specific to the chosen model. Production cross sections at the LHC also vary greatly, depending crucially on whether or not the new states carry color. Placing general bounds on electrically charged particles in this way is thus not an easy task. Moreover, for certain particles, the background can be large such that this type of search is not necessarily the most efficient one either.

In this paper we rather follow an alternative route, the one of precision physics. We use the fact that any of such new electrically charged particles contribute to the scattering of light-by-light. This happens through a loop as shown in figure 1. Contrary to LHC direct searches, light-by-light scattering amplitudes are fully characterized by the mass, spin and electric charge of the particle in the loop [3, 4]. This property offers a way to search for charged NP in a fully model-independent way.

In previous works [3, 4], such contributions were only included in an effective Lagrangian framework where they were matched to local effective operators of the type $F_{\mu\nu}^4$. The obvious drawback of this approach is that either one has to consider particles of masses much larger than the typical di-photon energy at the LHC — in which case the sensitivity is poor — or one has to introduce ad-hoc form-factors to mimic the unknown amplitude behaviour near the threshold. In this work we go beyond this effective operator approach, and consider the full one-loop amplitudes to light-by-light scattering from NP. This allows us to obtain reliable estimates for the LHC sensitivity for NP particles of any mass. In the high mass limit the results coincide with those obtained previously [4]. The one-loop amplitudes are implemented in the Forward Physics Monte Carlo (FPMC) generator [5] that we use in the simulation.

The SM quarks and leptons as well as the W boson also contribute to the light-by-light scattering via loops. One should notice that, at the LHC, typical di-photon energies are

JHEP02(2015)165

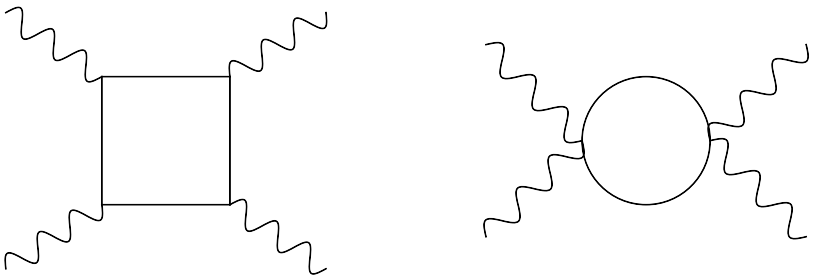

Figure 1. Typical diagrams of electrically charged particles contributing to light-by-light scattering.

much larger than the masses of these particles. However, while the fermion loop amplitudes approach constants at high energies, the W loop amplitude grows logarithmically [6]. It is therefore the main SM contribution to light-by-light scattering at the LHC whereas it is rarely included in the background simulations.

It is fairly surprising that prospects for studying light-by-light scattering are good at a hadron collider. This potential relies on the forward proton detectors that are planned to be built at about 220 m from the ATLAS main detector within the AFP project [7]. The CMS and TOTEM collaborations plan to use their forward proton detectors located at about the same position (CT-PPS project) [8]. Using these detectors, four-photon interactions can be detected with an unprecedented precision. Previous studies using proton-tagging at the LHC for New Physics searches can be found in refs. [3, 4, 9–19]. We refer to [20] for a study of light-by-light scattering at the LHC without proton tagging.

The outline of this paper is as follows. We first describe the exclusive di-photon production predicted by the Standard Model and discuss potential SM measurements at the LHC in section 2. In section 3 we detail new charged particles contributions to the four-photon amplitudes both in the simple decoupling limit as well as the full energy range. Sections 4 and 5 are dedicated to the forward proton detectors and the implementation of the simulation. Backgrounds and cuts for the simulation are detailed in section 6 and the expected sensitivity to new charged particles at the 14 TeV LHC is given is section 7. Finally, the reach on other new physics candidates inducing light-by-light scattering is discussed in section 8.

2 Standard Model exclusive di-photon production

2.1 Equivalent Photon Approximation

We use the the Equivalent Photon Approximation (EPA) [21, 22] to describe the two-photon production in pp collision. The almost real photons (with low virtuality $Q^2 = -q^2$) are emitted by the incoming protons producing an object X, $pp \to pXp$, through two-photon exchange $\gamma\gamma \to X$. The photon spectrum of virtuality Q^2 and energy E_γ is proportional to the Sommerfeld fine-structure constant α and reads:

$$dN = \frac{\alpha_{em}}{\pi}\frac{dE_\gamma}{E_\gamma}\frac{dQ^2}{Q^2}\left[\left(1-\frac{E_\gamma}{E}\right)\left(1-\frac{Q^2_{\min}}{Q^2}\right)F_E + \frac{E_\gamma^2}{2E^2}F_M\right] \tag{2.1}$$

JHEP02(2015)165

where E is the energy of the incoming proton of mass m_p, $Q^2_{\text{min}} \equiv m_p^2 E_\gamma^2/[E(E-E_\gamma)]$ the photon minimum virtuality allowed by kinematics and F_E and F_M are functions of the electric and magnetic form factors. They read in the dipole approximation [9, 22]

$$F_M = G_M^2 \qquad F_E = (4m_p^2 G_E^2 + Q^2 G_M^2)/(4m_p^2 + Q^2) \qquad G_E^2 = G_M^2/\mu_p^2 = (1 + Q^2/Q_0^2)^{-4} \tag{2.2}$$

The magnetic moment of the proton is $\mu_p^2 = 7.78$ and the fitted scale $Q_0^2 = 0.71\,\text{GeV}^2$. Since the electromagnetic form factors fall steeply as a function of Q^2, the two-photon cross section can be factorized into the sub-matrix element and the two photon fluxes. In order to obtain the production cross section, the photon fluxes are first integrated over Q^2

$$f(E_\gamma) = \int_{Q^2_{\text{min}}}^{Q^2_{\text{max}}} \frac{dN}{dE_\gamma dQ^2} dQ^2 \tag{2.3}$$

up to a sufficiently large value of $Q^2_{\text{max}} \approx 2$–$4\,\text{GeV}^2$. The result is given for instance in ref. [9].

The contribution to the integral above $Q^2_{\text{max}} \approx 2\,\text{GeV}^2$ is very small. The Q^2-integrated photon flux also falls rapidly as a function of the photon energy E_γ which implies that the two-photon production is dominant at small masses $W \approx 2\sqrt{E_{\gamma 1} E_{\gamma 2}}$. Integrating the product of the photon fluxes $f(E_{\gamma 1}) \cdot f(E_{\gamma 2}) \cdot dE_{\gamma 1} \cdot dE_{\gamma 2}$ from both protons over the photon energies while keeping the two-photon invariant mass fixed to W, one obtains the two-photon effective luminosity spectrum $dL^{\gamma\gamma}/dW$.

The production rate of massive objects via photon exchange at the LHC is however limited by the photon luminosity at high invariant mass. The integrated two-photon luminosity above $W > W_0$ for $W_0 = 23\,\text{GeV}$, $2 \times m_W \approx 160\,\text{GeV}$, and 1 TeV is respectively 1%, 0.15% and 0.007% of the luminosity integrated over the whole mass spectrum.

Using the effective relative photon luminosity $dL^{\gamma\gamma}/dW$, the total cross section reads

$$\sigma = \int \sigma_{\gamma\gamma \to X} \frac{dL^{\gamma\gamma}}{dW} dW \tag{2.4}$$

where $\sigma_{\gamma\gamma \to X}$ denotes the cross section of the sub-process $\gamma\gamma \to X$, dependent on the invariant mass of the two-photon system.

In these studies, we assume both protons to be intact after interaction. Additional soft gluon exchanges between the two protons might destroy the protons. A traditional way to take this effect into account is to introduce the so-called survival probability that the protons remain intact [23, 24] in γ induced processes. In our studies, we assumed a survival probability of about 90%. More recent studies [25] show that this might be slightly optimistic and the survival probability at high di-photon masses might be of the order of 60%. In that case, the yield should be reduced accordingly. It is thus important to measure that quantity at the LHC.

2.2 Standard Model exclusive di-photon production

The Standard Model predicts exclusive di-photon production with two intact protons through various processes, which can be decomposed in two parts, as shown in figure 2.

JHEP02(2015)165

The first diagram (figure 2, left) corresponds to exclusive QCD di-photon production via gluon exchanges [23] (the second gluon ensures that the exchange is colorless leading to intact protons in the final state) and the second one (figure 2, right) via photon exchanges.

It is worth noticing that quarks, leptons and W-boson loops plus the associated interference terms need to be considered in order to get the correct SM cross section. These loops have been computed in refs. [6, 26–28]. We collect explicit expressions in appendix A. The various contributions are illustrated in figure 3, where we display the integrated cross sections of the different exclusive di-photon processes varying the requirement on the minimum mass of the photon pair. Both photons are required to have a transverse momenta above 10 GeV. We can see that the QCD induced processes are dominant at low di-photon mass whereas the photon induced ones (QED processes) dominate at higher masses. The quark and lepton loops contribution is the second leading one, whereas the W loop contribution dominates at high di-photon masses and starts getting over the QCD contribution as of a di-photon mass of ∼100 GeV. The W-loop contribution is omitted in most of the studies and it is one of the first times that all terms (including interference) are implemented in a single MC generator, FPMC.

In table 1, we report a few values of the cross sections from figure 3 discussed above. The threshold where the W-loop contribution starts dominating the production is for a di-photon mass slightly above 100 GeV as we already mentioned. A low mass measurement of the gluon contribution would be possible at the LHC in the case of the special runs at low luminosity and low pile up ($\mu \sim 1-2$) with modified optics ($\beta^* = 90$ m), currently being discussed among the different LHC experiments [29]. The intact protons would be detected in the vertical roman pots of the TOTEM or ALFA detectors. Thanks to the low instantaneous luminosity of those special runs one should be able to implement a dedicated di-photon trigger with p_T thresholds as low as $p_{T1,2} > 5$ GeV, and following table 1, a di-photon mass requirement of $m_{\gamma\gamma} >$10 GeV would lead to a sizeable cross section of 372.1 fb. For a typical integrated luminosity of 0.1 fb^{-1} expected in these special runs, which corresponds approximately to a week of data taking, 37 events can be measured and compared to the different exclusive di-photon cross section calculation and to the previous and unique measurement of this process done by the CDF collaboration [30].

On the other hand, the Standard Model QED production does not seem to be reachable at the LHC in pp collisions. It might be possible to study the di-photon production via quark, lepton and even W loops at the LHC in the heavy ion mode [20, 31].

3 Effects of new charged particles on exclusive di-photon production

3.1 General considerations

The particles running in the loops in figure 1 are characterized by their electric charge Q, their spin S, and their mass m. The loop amplitude is proportional to $\alpha_{\rm em}^2 Q^4$.

However, the new particles also have in general a multiplicity with respect to electromagnetism. For instance, the multiplicity is three if the particles are colored. One can

JHEP02(2015)165

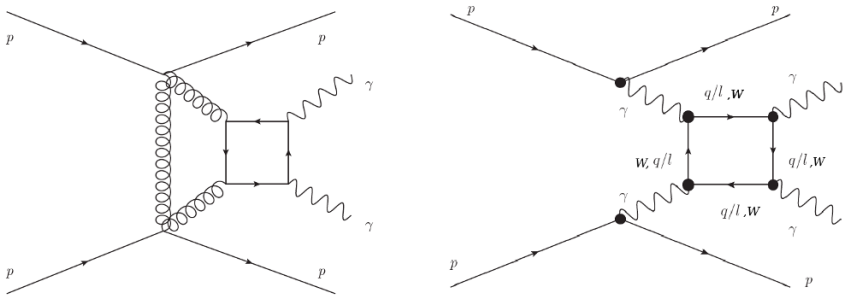

Figure 2. Feynman diagrams predicted by the Standard Model leading to the exclusive production of two photons and two intact protons in the final state at the lowest order of perturbation theory.

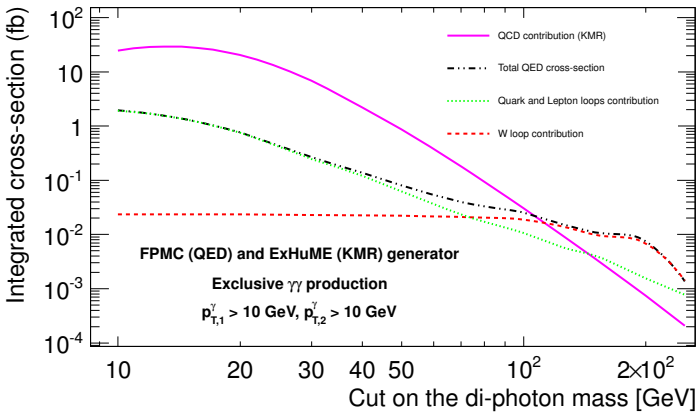

Figure 3. Integrated cross sections of the different exclusive di-photon processes with intact protons at the 13 TeV LHC, plotted against the required minimum di-photon mass. Both photons are required to have a transverse momentum above 10 GeV.

Cut / Process	QCD Exclusive (KMR)	QED Fermion loop	W loop
$m_{\gamma\gamma} > 10\,\text{GeV}, p_{T1,2} > 5\,\text{GeV}$	372.1 fb	4.71 fb	0.024 fb
$m_{\gamma\gamma} > 10\,\text{GeV}, p_{T1,2} > 10\,\text{GeV}$	24.2 fb	1.87 fb	0.023 fb
$m_{\gamma\gamma} > 20\,\text{GeV}, p_{T1,2} > 10\,\text{GeV}$	20.4 fb	0.75 fb	0.023 fb
$m_{\gamma\gamma} > 50\,\text{GeV}, p_{T1,2} > 10\,\text{GeV}$	0.87 fb	0.061 fb	0.022 fb
$m_{\gamma\gamma} > 100\,\text{GeV}, p_{T1,2} > 10\,\text{GeV}$	0.030 fb	0.015 fb	0.019 fb
$m_{\gamma\gamma} > 200\,\text{GeV}, p_{T1,2} > 10\,\text{GeV}$	7.4e-4 fb	$1.5{\cdot}10^{-3}$ fb	9.7e-3 fb
$m_{\gamma\gamma} > 500\,\text{GeV}, p_{T1,2} > 10\,\text{GeV}$	3.2e-6 fb	$< 5.0{\cdot}10^{-4}$ fb	1.4e-3 fb

Table 1. Integrated cross sections of the different SM exclusive di-photon production processes at the LHC at $\sqrt{s} = 14\,\text{TeV}$ for various requirements on the di-photon mass ($m_{\gamma\gamma}$) and photon transverse momenta ($p_{T1,2}$).

JHEP02(2015)165

simply take into account this multiplicity by defining

$$Q_{\rm eff}^4 = \mathrm{tr}\, Q^4 \tag{3.1}$$

where the trace goes over all particles with the same approximate mass. The amplitude then becomes proportional to

$$\mathcal{M} \propto \alpha_{\rm em}^2 Q_{\rm eff}^4 \,. \tag{3.2}$$

As an example, consider the minimal composite Higgs models with global symmetry group $G = \mathrm{SO}(5) \times \mathrm{U}(1)_X$ [1]. The simplest and most common choices for the embeddings of the quark partners are the $5_{\frac{2}{3}}$ or $14_{\frac{2}{3}}$ representations of G. After the breaking $G \to H = \mathrm{SU}(2)_L \times \mathrm{SU}(2)_R \times \mathrm{U}(1)_X$ the theory predicts light vector-like (VL) fermions in the $(1,1)_{\frac{2}{3}}$, $(2,2)_{\frac{2}{3}}$ or $(3,3)_{\frac{2}{3}}$ representations. The latter two actually contain states of various electric charges which are approximately degenerate in mass. One then obtains[1]

$$\begin{aligned} Q_{\rm eff} &= 2.22 \qquad (2,2) \text{ representation} \\ Q_{\rm eff} &= 3.80 \qquad (3,3) \text{ representation} \end{aligned} \tag{3.3}$$

which in particular contain the multiplicity due to color. For larger global groups the effective charges can become even larger, as several of the above mentioned representations can occur simultaneously. There is in principle no reason to restrict to the smallest group SO(5) and to the smallest representations mentioned above, other than simplicity and minimality. Larger representations raise the effective charge more efficiently than going to larger groups.

Various bounds on VL quarks from direct searches already exist. VL quarks mixing strongly with third generation quarks ("top/bottom partners") are most strongly constrained and yield bounds of the order of $400 - 700\,\mathrm{GeV}$, depending on the branching ratios. Bounds are generally weaker for VL quarks mixing with lighter generations [32]. To the best of our knowledge there are not yet any bounds on VL leptons, which are equally predicted in many of these models. Note that VL leptons have much smaller production cross sections at the LHC.

Summarizing, while direct searches already constrain quite a lot the parameter space of specific models with VL quarks, it is difficult to extract completely model independent bounds, and some assumptions about specific couplings/mixings or branching fractions are required. On the other hand, our results will be expressed in terms of mass, spin and effective charge $Q_{\rm eff}$, and any specific model can be easily mapped onto these quantities.

3.2 Effective Field Theory (EFT)

In the limit where the mass of the new charged particle is large with respect to the energy of the process, $m \gg E$, one can describe the four-photon interactions using higher-dimensional local operators in an effective Lagrangian,

$$\mathcal{L}_{4\gamma} = \zeta_1 F_{\mu\nu} F^{\mu\nu} F_{\rho\sigma} F^{\rho\sigma} + \zeta_2 F_{\mu\nu} F^{\nu\rho} F_{\rho\lambda} F^{\lambda\mu} \,. \tag{3.4}$$

[1]The effective charges are dominated by the states of highest charge in each case, which are a single $Q = \frac{5}{3}$ ($Q = \frac{8}{3}$) state in the case of the $(2,2)$ and $(3,3)$ respectively.

JHEP02(2015)165

These are operators of dimension 8. The coefficients ζ_1, ζ_2, although they can be studied separately as in the previous work [4], are ultimately both predicted by any model of New Physics. From the effective Lagrangian eq. (3.4) one can compute the unpolarized four-photon angular cross section

$$\frac{d\sigma}{d\Omega} = \frac{1}{16\pi^2\, s}(s^2+t^2+st)^2\left[48(\zeta_1)^2+40\zeta_1\zeta_2+11(\zeta_2)^2\right] \tag{3.5}$$

where s, t are the usual Mandelstam variables. Since the amplitudes interfere with the background (e.g. the W loops), eq. (3.5) is valid at sufficiently large s or ζ_i. Let us stress that eq. (3.5) only relies on the effective Lagrangian eq. (3.4) and makes no reference to the origin of the coefficients ζ_i.

As the EFT is nonrenormalizable, at high energies one expects a breakdown of unitarity. Using the well-known partial wave analysis [33] we can estimate for what values of ζ_i and s the theory remains unitary. By imposing unitarity on the S-wave of the EFT amplitudes in eq. (C.2) one finds the conditions

$$(4\zeta_1+3\zeta_3)s^2 < 4\pi\,, \qquad (4\zeta_1+\zeta_2)s^2 < \frac{12}{5}\pi\,, \tag{3.6}$$

for the $\mathcal{M}_{++++}$ and $\mathcal{M}_{++--}$ amplitudes respectively. As most of the recorded diphoton events have $\sqrt{s}$ below 1 TeV (see figure 5), we expect the EFT to remain unitary for couplings up to

$$\zeta_i \lesssim (10^{-12}-10^{-11})\ \mathrm{GeV}^{-4}\,. \tag{3.7}$$

The sensitivities we will derive in section 7.1 are much better than these unitarity bounds. However, we remark that unless the underlying New Physics model is very strongly coupled, the condition $m < E$ provides a stronger constraint on the ζ_i and EFT typically breaks down before unitarity is violated. Condition (3.7) should thus be considered as an absolute model-independent upper bound above which we no longer can trust the EFT approximation.

We now return to the case of new electrically charged particles with arbitrary spin S. Using the background field method as in the general computation of [3], we obtain the following expression for the coefficients of the 4γ operators,

$$\zeta_i = \frac{\alpha_{\mathrm{em}}^2 Q_{\mathrm{eff}}^4}{m^4}\, c_{i,S}\,, \tag{3.8}$$

where

$$c_{1,S} = \begin{cases} \dfrac{1}{288} & S=0 \\ -\dfrac{1}{36} & S=\frac{1}{2} \\ -\dfrac{5}{32} & S=1 \end{cases}, \quad c_{2,S} = \begin{cases} \dfrac{1}{360} & S=0 \\ \dfrac{7}{90} & S=\frac{1}{2} \\ \dfrac{27}{40} & S=1 \end{cases}. \tag{3.9}$$

The contributions from the scalar are smaller by one order of magnitude with respect to the fermion and vector. It can easily be checked that in the case of fermions $\mathcal{L}_{4\gamma}$ reduces to the famous Euler-Heisenberg Lagrangian [34].

JHEP02(2015)165

One may observe that the magnitude of the contributions to light-by-light scattering grows fast with the spin — see eq. (3.9). This intriguing fact suggests that contributions from higher-spin particles might be particularly large. Higher-spin states potentially emerge in many extensions of the Standard Model. This includes the composite states arising from a new strongly-interacting gauge sector, as well as low-energy strings (see [35] for a recent review). A naive estimate using the background field method suggests that higher-spin contributions would go as $\zeta_i \propto S^5$. However this result cannot be fully trusted, because higher-spin Lagrangians intrinsically contain higher-dimensional interactions that lead to extra-divergences in the loops. The tools necessary for higher-spin phenomenology are not yet available, and are under development [36].

3.3 Exact amplitudes

The effective field theory analysis has the advantage of being very simple. However it is only valid as long as the center-of-mass energy is small with respect to the threshold of pair-production of real particles, $s \ll 4m^2$. Since the maximum proton missing mass (corresponding to the di-photon invariant mass in our case) is of the order of $\sim 2\,\text{TeV}$ at the 14 TeV LHC, for particles lighter than $\sim 1\,\text{TeV}$ the effective field theory computation needs to be corrected. This can be done by using ad-hoc form factors, as often done in the literature.

The more correct approach is to take into account the full momentum dependence of the four-photon amplitudes. They have been computed in the case of fermions in ref. [28] and for vector bosons in ref. [6]. Next-to-leading order corrections from QED and QCD are found to be negligible in [37].

Following the notation and normalization of ref. [28], the unpolarized cross section can be expressed in terms of the various helicity configurations as

$$\frac{d\sigma}{d\Omega} = \frac{\alpha_{\text{em}}^4 Q_{\text{eff}}^8}{2\pi^2 s}\left(|\mathcal{M}_{++++}|^2 + |\mathcal{M}_{++--}|^2 + |\mathcal{M}_{+-+-}|^2 + |\mathcal{M}_{+--+}|^2 + 4|\mathcal{M}_{+++-}|^2\right) \tag{3.10}$$

Due to the relations

$$\begin{aligned}\mathcal{M}_{+-+-}(s,t,u) &= \mathcal{M}_{++++}(u,t,s)\,,\\ \mathcal{M}_{+--+}(s,t,u) &= \mathcal{M}_{++++}(t,s,u)\end{aligned} \tag{3.11}$$

only the configurations $\mathcal{M}_{++++}$, $\mathcal{M}_{++--}$ and $\mathcal{M}_{+++-}$ have to be computed. We summarize them in appendix A together with various kinematical limits that are useful both for theoretical as well as numerical considerations. For comparison, we give in appendix C the same amplitudes as obtained from the effective Lagrangian eq. (3.4). All those amplitudes were implemented into a single MC generator dedicated to forward physics, the Forward Physics Monte Carlo Generator.

4 The forward proton detectors

In this study, the protons are assumed to be detected in the ATLAS Forward Proton (AFP) detector at 206 (AFP1 detector) and 214 (AFP2 detector) meters on both sides of

JHEP02(2015)165

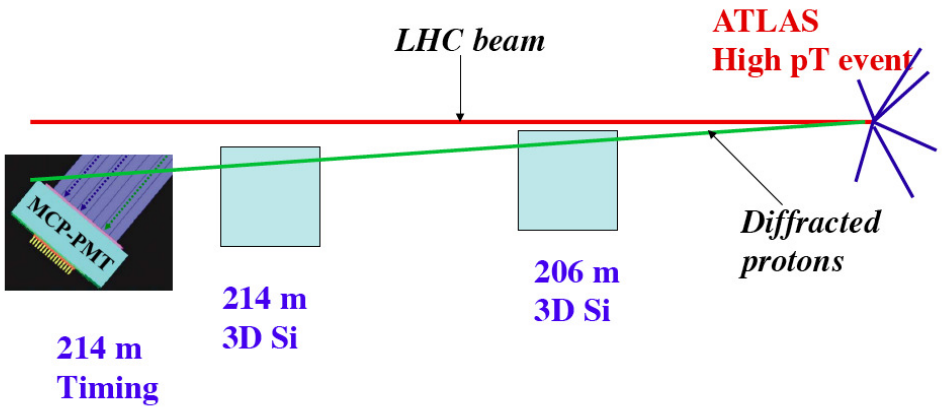

Figure 4. Scheme of the AFP detector. Roman pot hosting Si and timing detectors will be installed on both sides of ATLAS at 206 and 214 m from the ATLAS nominal interaction point. The CMS-TOTEM collaborations will have similar detectors.

the ATLAS experiment [7] (see figure 4) or in a similar detector proposed by the TOTEM and CMS collaborations, the so called CT-PPS detector, to be installed on both sides of the CMS detector.

In AFP1, a tracking station composed by 6 layers of Silicon detectors will be deployed. The second section, AFP2, will contain a second identical tracking station and a timing detector. Likewise, the CT-PPS of CMS will also use the same combination of tracking and timing detectors, with the far station using specially designed cylindrical roman pots to house the timing detectors [38].

The proton taggers are expected to determine the fractional proton momentum loss ξ in the range $0.015 < \xi < 0.15$ with a relative resolution of 2%. This leads to the acceptance in di-photon mass shown in figure 5 between about 350 and 1700 GeV [7]. In addition, the time-of-flight of the protons can be measured within 10 ps, which translates into 2.1 mm resolution on the determination of the interaction point along the beam axis z. In the following, we always assume both intact protons in the final state to be tagged in AFP or CT-PPS.

5 Setup of the simulation

5.1 Event generation with the Forward Physics Monte Carlo Generator

The Forward Physics Monte Carlo Generator was designed to produce single diffractive, double pomeron exchange (DPE), exclusive diffractive and photon-induced processes within the same framework. We use FPMC to produce all diffractive and photon induced events, the diffractive and exclusive processes are implemented by modifying the HERWIG [39] routine for the $e^+e^- \to (\gamma\gamma) \to X$ process. In case of the two-photon pp events, the Weizsäcker-Williams (WWA) formula describing the photon emission off point-like electrons is substituted by the Budnev flux [22] which describes properly the coupling of the photon to the proton, taking into account the proton electromagnetic structure. For the

JHEP02(2015)165

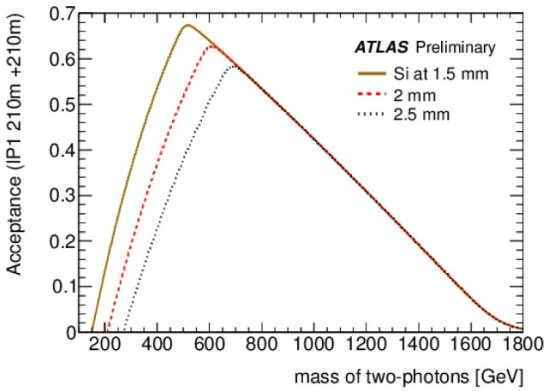

Figure 5. Di-photon mass acceptance for the AFP detectors for the LHC nominal running at $\beta^* = 0.6$ m.

central exclusive production, a look-up table of the effective gluon-gluon luminosity computed by ExHuME [40] is implemented. In case of the pomeron/reggeon exchange, the WWA photon fluxes are turned to the pomeron/reggeon fluxes multiplied by the diffractive parton density functions.

For processes in which the partonic structure of the pomeron is probed, the existing HERWIG matrix elements of non-diffractive production are used to calculate the production cross sections. The parton distributions in the Pomeron as determined by the H1 collaboration at HERA (see [41] an references therein) are used with a survival probability of 0.03 [23, 24]. The list of particles is corrected at the end of each event to change the type of particles from the initial state electrons to hadrons and from the exchanged photons to pomerons/reggeons, or gluons, depending on the process.

5.2 Background simulation and event reconstruction

In an experiment like ATLAS or CMS, the photons can be reconstructed in the central detectors, instrumented with electromagnetic calorimeters covering the pseudorapidity range $|\eta| \lesssim 2.5$. The calorimeters provide excellent energy and position resolution, $\Delta E/E$ around 1% for energies above few hundred GeV, $\Delta\eta \sim 0.001$ and $\Delta\phi \sim 1$ mrad to few mrad. For transverse momenta in the range of few tens of GeVs up to about 1 TeV and even in the presence of 100 additional collisions occurring in the same or neighbouring bunch crossings (pile up), the photon identification efficiency is expected to be around 75% with jet rejection factors in excess of 4000 [42]. In addition, about 1% of the electrons are misidentified as photons. These numbers are for the ATLAS detectors but similar sensitivities are expected for CMS.

A significant fraction of the photons convert to electron-positron pairs in the material upstream the calorimeters. In the region instrumented with silicon tracking detectors the material budget greatly varies as a function of η in both experiments, typically between less than 0.5 radiation lengths (X_0) at $\eta = 0$ up to 2 X_0 at higher η. As a result, about 15-30% of the photons convert in this region. The charged tracks associated contribute to the fake electron to photon rates that can reach 1% and on the other hand can help locating the

JHEP02(2015)165

interaction point with sub-millimiter accuracy. An alternative method exploits the longitudinal segmentation of the ATLAS electromagnetic calorimeter to determine the photon production point along the beam axis within ~ 15 mm. By locating precisely the interaction point one can measure the photon trajectory and, in combination with the proton detectors, determine the four momenta of all particles in the final state. The constraint of the full event kinematics is an extremely powerful feature to reject the backgrounds where two photons are produced by a hard scattering process and two intact protons arise from pile up interactions.

The analysis was designed to yield high signal selection efficiency and suppress the backgrounds that are divided into three classes. Exclusive processes with two intact photons and a pair of photon candidates include the SM light-by-light scattering, the central-exclusive production of two photons via two-gluon exchange and $\gamma\gamma \to e^+e^-$. Processes involving double pomeron exchange can result in protons accompanied by two jets, two photons and a Higgs boson that decay into two photons. Finally, one can have gluon or quark-initiated production of two photons, two jets or two electrons (Drell-Yan) with intact protons arising from pile up interactions. Both the anomalous $\gamma\gamma \to \gamma\gamma$ signal, exclusive and DPE background processes were simulated by the FPMC generator, with the exception of the central exclusive production of $\gamma\gamma$ that was simulated using ExHuME.

6 Event selection

The number of expected signal and background events after each cut is given in table 2 for an integrated luminosity of 300 fb^{-1} ($\simeq$ 3 years of data-taking at the LHC run 2) and 50 pile up interactions for a center-of-mass energy of 14 TeV. We fix $S = 1$, $Q_{\text{eff}} = 4$, $m = 340$ GeV, and the associated results from EFT are also given for comparison. As expected, the full amplitude calculation lies between the EFT prediction with and without form factor (f.f.), defined as f.f. $= 1/(1 + (m^2_{\gamma\gamma}/\Lambda')^2)$ with $\Lambda' = 1$ TeV. The discrepancy appears because the EFT is not valid for such low mass (see section 3 and figure 8). The backgrounds originate from di-photon and di-electron exclusive production, di-photon and di-jet production via double Pomeron exchanges, SM di-photon production with pile up, and SM di-jet and di-electron production with pile up where the jets or electrons are misidentified as photons.

The different cuts follow the analysis presented in ref. [4]. Gaussian smearings of 1% for the total energy, 0.001 for the pseudorapidity and 1 mrad for the azimuthal angle are applied to each photon. The di-photon mass distribution is given in figure 6 for the signal and the different backgrounds. The signal appears at high di-photon masses whereas the SM background stands at low masses. The first cuts requires that both protons are measured in AFP or CT-PPS ($0.015 < \xi < 0.15$) and the photons are produced at high p_T and high mass ($p_{T1,2} > 200,\ 100$ GeV and $m_{\gamma\gamma} > 600$ GeV). After those requirements, the SM exclusive background (dominated by the QED W-loop contribution) is very small (typically 0.2 events). The main remaining background is the SM di-photon production associated with intact protons from pile up. In order to suppress this background, the signal event topology is used, requiring that photons are emitted back-to-back and with

JHEP02(2015)165

Cut / Process	Signal (full)	Signal with (without) f.f (EFT)	Excl.	DPE	DY, di-jet + pile up	$\gamma\gamma$ + pile up
$[0.015 < \xi_{1,2} < 0.15,$ $p_{T1,(2)} > 200, (100)\,\text{GeV}]$	130.8	36.9 (373.9)	0.25	0.2	1.6	2968
$m_{\gamma\gamma} > 600\,\text{GeV}$	128.3	34.9 (371.6)	0.20	0	0.2	1023
$p_{T2}/p_{T1} > 0.95,$ $\lvert\Delta\phi\rvert > \pi - 0.01]$	128.3	34.9 (371.4)	0.19	0	0	80.2
$\sqrt{\xi_1\xi_2 s} = m_{\gamma\gamma} \pm 3\%$	122.0	32.9 (350.2)	0.18	0	0	2.8
$\lvert y_{\gamma\gamma} - y_{pp}\rvert < 0.03$	119.1	31.8 (338.5)	0.18	0	0	0

Table 2. Number of signal events for $S = 1$, $Q_{\text{eff}} = 4$, $m = 340\,\text{GeV}$ and background events after various selections for an integrated luminosity of 300 fb^{-1} and $\mu = 50$ at $\sqrt{s} = 14\,\text{TeV}$. Values obtained using the corresponding EFT couplings with and without form factors are also displayed. At least one converted photon is required. Excl. stands for exclusive backgrounds and DPE for double pomeron exchange backgrounds (see text).

similar p_T. Further requirements on the exclusivity of the events as shown in figure 7 using the forward proton detectors (the di-photon mass and rapidity are equal within detector resolution when it is computed using the di-photon in ATLAS/CMS central detector or the proton information from CT-PPS/AFP) completely suppress the remaining background, while the signal efficiency is over 70%. One should notice that tagging the protons is absolutely fundamental to suppress the $\gamma\gamma$ + pile up events. Without the forward proton detector measurements, the number of signal events (34.9) would be much smaller than the number of background pile up events (80.2). Further background reduction is even possible by requiring the photons and the protons to originate from the same vertex by measuring their time-of-flight that provides an additional rejection factor of 40 for 50 pile up interactions, if one assumes a timing resolution of 10 ps, showing the large margin on the background suppression. A similar study at a higher pile up of 200 was performed and led to a very small background (< 5 expected background events for 300 fb^{-1} without re-optimizing the event selection), showing the robustness of this analysis. Moreover, if one relaxes the request of at least one photon to be converted, the signal is increased by a factor 3 to 4. In comparison with the results given in ref. [4], we added the SM di-photon background induced by W loops, and the signal has increased by a factor ~ 2.1.[2]

7 Expected sensitivity for charged particles at the 14 TeV LHC

In this section, we present the estimates for the LHC sensitivities to new massive charged particles obtained through our proposed measurement of light-by-light scattering. Results

[2]Our previous estimate was relying on the COMPHEP software [43, 44] interfaced with FPMC. For this work we implemented directly eq. (3.5) in FPMC. We verified that the cross section computed from the full amplitudes reduces to the EFT limit at low energies, providing an independent cross-check of the implementation.

JHEP02(2015)165

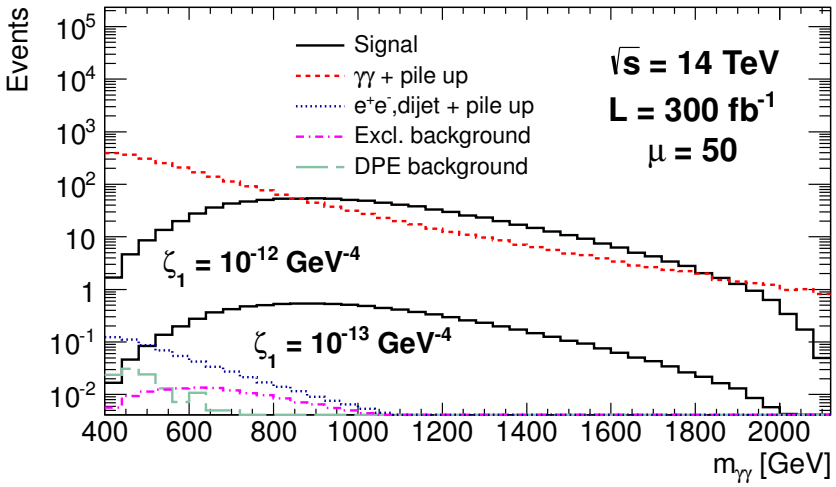

Figure 6. Di-photon invariant mass distribution for the signal considering two different coupling values (10^{-12} and 10^{-13} GeV^{-4}, see eq. (3.4)) and for the backgrounds (dominated by $\gamma\gamma$ with protons from pile up), requesting two intact protons in the forward detectors and two photons in the central detector with a minimun p_{T} of 200 (100) GeV for the leading (subleading) photon. The considered integrated luminosity is 300 fb^{-1} and the pile up $\mu = 50$. Excl. stands for exclusive backgrounds and DPE for double pomeron exchange backgrounds (see text).

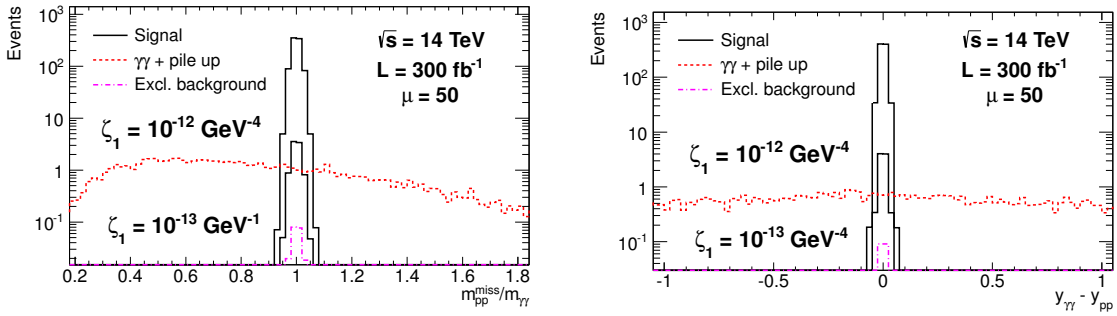

Figure 7. Di-photon to missing proton mass ratio (left) and rapidity difference (right) distributions for signal considering two different coupling values (10^{-12} and 10^{-13} GeV^{-4}, see eq. (3.4)) and for backgrounds after requirements on photon p_{T}, di-photon invariant mass, p_{T} ratio between the two photons and on the angle between the two photons. At least one converted photon is required. The integrated luminosity is 300 fb^{-1} and the average pile up is $\mu = 50$.

are provided both in the EFT framework and using full loop amplitudes. Both approaches coincide in the decoupling limit $m \gg E$.

7.1 EFT results

We first present the sensitivities for the effective four-photon couplings ζ_i. These sensitivities are given in table 3 for different scenarios corresponding to the medium luminosity at the LHC (300 fb^{-1}) and the high luminosity (3000 fb^{-1} in ATLAS), with and without an ad-hoc form factor [4] with a cutoff at 1 TeV. We give the 5σ discovery potential as well as the 95% CL limits with a pile up of 50, and requesting or not at least one photon to be converted.

JHEP02(2015)165

Luminosity	300 fb^{-1}	300 fb^{-1}	300 fb^{-1}	300 fb^{-1}	3000 fb^{-1}
pile up (μ)	50	50	50	50	200
coupling	≥ 1 conv. γ	≥ 1 conv. γ	all γ	all γ	all γ
(GeV^{-4})	5 σ	95% CL	5 σ	95% CL	95% CL
ζ_1 f.f.	$8 \cdot 10^{-14}$	$5 \cdot 10^{-14}$	$4.5 \cdot 10^{-14}$	$3 \cdot 10^{-14}$	$2.5 \cdot 10^{-14}$
ζ_1 no f.f.	$2.5 \cdot 10^{-14}$	$1.5 \cdot 10^{-14}$	$1.5 \cdot 10^{-14}$	$9 \cdot 10^{-15}$	$7 \cdot 10^{-15}$
ζ_2 f.f.	$2 \cdot 10^{-13}$	$1 \cdot 10^{-13}$	$9 \cdot 10^{-14}$	$6 \cdot 10^{-14}$	$4.5 \cdot 10^{-14}$
ζ_2 no f.f.	$5 \cdot 10^{-14}$	$4 \cdot 10^{-14}$	$3 \cdot 10^{-14}$	$2 \cdot 10^{-14}$	$1.5 \cdot 10^{-14}$

Table 3. $5\,\sigma$ discovery and 95% CL exclusion limits on ζ_1 and ζ_2 couplings in GeV^{-4} (see eq. (3.4)) with and without form factor (f.f.), requesting at least one converted photon (≥ 1 conv. γ) or not (all γ). All sensitivities are given for 300 fb^{-1} and $\mu = 50$ pile up events (medium luminosity LHC) except for the numbers of the last column which are given for 3000 fb^{-1} and $\mu = 200$ pile up events (high luminosity LHC).

In the table we provide only the sensitivities for ($\zeta_1 \neq 0$, $\zeta_2 = 0$) and ($\zeta_1 = 0$, $\zeta_2 \neq 0$). It turns out that with the cuts adopted in our analysis (see section 6), the interference of the ζ_i vertices with the background is negligible. The cross section has thus the form given in eq. (3.5) to a good approximation. Knowing the sensitivity for a given value of ζ_1, ζ_2, it is straightforward to recast it in the complete (ζ_1, ζ_2) plane, where it defines an ellipse

$$\zeta^2 \equiv \; 48(\zeta_1)^2 + 40\zeta_1\zeta_2 + 11(\zeta_2)^2 \,. \tag{7.1}$$

We find that the sensitivity extends up to $|\zeta| \approx 6 \cdot 10^{-14}\,\text{GeV}^{-4}$.

Using a form factor with higher cutoff $\gtrsim 2$ TeV leads to similar results as without form factors. The reach is slightly better than in our previous study [4] because of the increase of the number of signal events (see footnote 2). The obvious inconvenience of the EFT approach is that it is valid only in the high mass region, $m \gg E$. In order to use the EFT result down to $m \sim E$, it is common to introduce ad-hoc form factors which mimics the behaviour of the — unknown — amplitudes near the threshold. Clearly, this method introduces a great deal of arbitrariness into the results. Not only do the results depend on the functional form of the form factor, but also on the energy scale at which they are introduced.

7.2 Results from exact amplitudes

This section contains our more general results for charged particles. Contrary to the EFT approach which is valid on in the decoupling limit and requires ad-hoc form factors to be valid near the threshold, the use of the full amplitudes provides exact results for any mass.

The results are given in table 4 and figure 8 where we display the 5σ discovery, 3σ evidence and 95% C.L. limit for fermions and vectors for a luminosity of 300 fb^{-1} and a pile up of 50. We find that a vector (fermion) with $Q_{\text{eff}} = 4$, can be discovered up to mass $m = 700\,\text{GeV}$ (370 GeV). At high mass, the exclusion bounds follow isolines $Q \propto m$, as dictated by the EFT couplings eq. (3.8). Extrapolating the same analysis to a higher

JHEP02(2015)165

Mass (GeV)	300	600	900	1200	1500
Q_{eff} (vector)	2.2	3.4	4.9	7.2	8.9
Q_{eff} (fermion)	3.6	5.7	8.6	—	—

Table 4. $5\,\sigma$ discovery limits on the effective charge of new generic charged fermions and vectors for various masses scenarios in the case of no requirement of photon conversion at the analysis stage and full integrated luminosity at the medium-luminosity LHC (300 fb^{-1}, $\mu = 50$).

luminosity of 3000 fb^{-1} for a pile up of 200 leads to a slighlty improved sensitivity of $m = 740\,\text{GeV}$ (410 GeV) for vectors (fermions).

Comparing with our discussion in section 3.1, one notices that some searches for VL quarks, as motivated from e.g. Composite Higgs models, already lead to stronger bounds than the ones projected here. For instance, VL top partners arising from the $(2, 2)$ (corresponding to $Q_{\text{eff}} \approx 2.2$) of mass $m = 500\,\text{GeV}$ would be excluded from present LHC data, while they would be out of reach in our method. On the other hand, our results are completely model-independent. They apply just as well to different effective charges, are independent of the amount of mixing with the SM quarks, and even apply to VL leptons.

7.3 Comparison with the muon $g - 2$ measurement

Finally we would like to comment on the possibility to observe charged particles in other precision observables. For instance, they could contribute to the magnetic dipole moment of the muon via a higher-loop diagrams as shown in figure 9.[3] The contribution to the coefficient of the effective dipole operator $F_{\mu\nu}\bar{\mu}_L\sigma^{\mu\nu}\mu_R$, up to $\mathcal{O}(1)$ numbers and factors of $\log(m_\mu/m)$ can be estimated as[4]

$$d_\mu^{(2-\text{loop})} \sim \frac{e^5 Q_{\text{eff}}^2 m_\mu}{m^2 (16\pi^2)^2}\,, \qquad d_\mu^{(3-\text{loop})} \sim \frac{e^7 Q_{\text{eff}}^4 m_\mu}{m^2 (16\pi^2)^3} \tag{7.2}$$

leading to contributions to $a_\mu = 4\, d_\mu m_\mu / e$ of the order of

$$\begin{aligned} \Delta a_\mu^{(2)} &\sim 1.5 \cdot 10^{-12} \left(\frac{100\ \text{GeV}}{m}\right)^2 Q_{\text{eff}}^2\,, \\ \Delta a_\mu^{(3)} &\sim 8.6 \cdot 10^{-16} \left(\frac{100\ \text{GeV}}{m}\right)^2 Q_{\text{eff}}^4\,. \end{aligned} \tag{7.3}$$

Unless the effective charge is extremely large we can focus on just the two-loop contribution. The current experimental uncertainty for a_μ is around $\sim 6 \cdot 10^{-10}$, implying a sensitivity of this measurement to $m/Q_{\text{eff}} \sim 5\,\text{GeV}$. Comparing this estimate to our projections from figure 8 we see that, despite its impressive accuracy, the $g - 2$ measurement is not competitive with our method.

[3] We would like to thank O. Lebedev for suggesting this possibility.

[4] Strictly speaking, the two-loop graph is proportional to $\text{tr}\, Q^2$ and not to $Q_{\text{eff}}^2 = (\text{tr}\, Q^4)^{\frac{1}{2}}$. We ignore this small difference as we are content with a rough estimate here.

JHEP02(2015)165

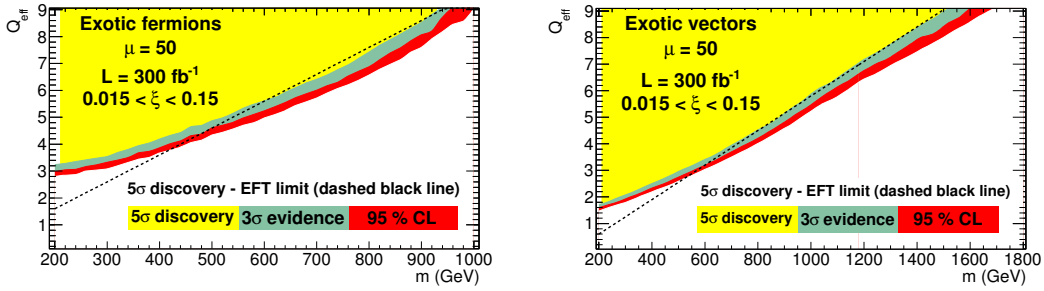

Figure 8. Exclusion plane in terms of mass and effective charge of generic fermions and vectors in the case of no requirement of photon conversion at the analysis stage and full integrated luminosity at the medium-luminosity LHC (300 fb^{-1}, $\mu = 50$).

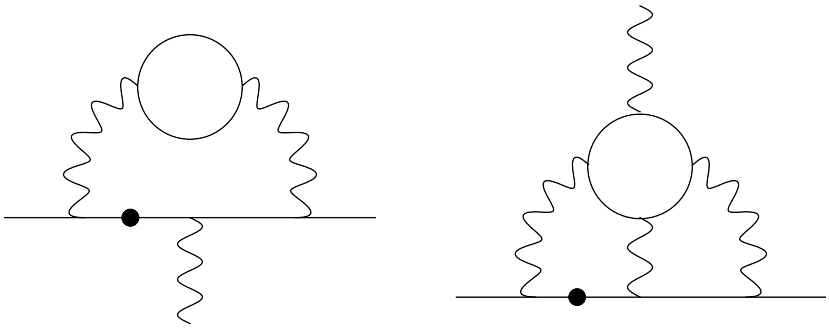

Figure 9. Two and three loop contribution to the muon anomalous gyromagnetic factor. The dot represents a muon mass insertion and the circle a generic NP particle of mass m and charge Q_{eff}.

8 Neutral contributions to light-by-light scattering

In the decoupling limit, any new physics contribution can be mapped onto the (ζ_1, ζ_2) plane. This provides a model-independent way to compare and summarize the discovery reach for various candidates. The EFT mapping for charged particles has been discussed in section 3.2. Beyond perturbative contributions to ζ_i^γ from charged particles, non-renormalizable interactions of neutral particles are also present in common extensions of the SM. Such theories can contain scalar, pseudo-scalar and spin-2 resonances, respectively denoted by φ, $\tilde{\varphi}$ and $h^{\mu\nu}$. Independently of the particular New Physics model they originate from, their leading couplings to the photon are fixed completely by Lorentz and CP symmetry as

$$\begin{aligned}\mathcal{L}_{\gamma\gamma} = f_{0^+}^{-1}\,\varphi\,(F_{\mu\nu})^2 + f_{0^-}^{-1}\,\tilde{\varphi}\,F_{\mu\nu}F_{\rho\lambda}\,\epsilon^{\mu\nu\rho\lambda} \\ + f_2^{-1}\,h^{\mu\nu}\,(-F_{\mu\rho}F_\nu{}^\rho + \eta_{\mu\nu}(F_{\rho\lambda})^2/4)\,,\end{aligned} \tag{8.1}$$

where the f_S have mass dimension 2. They then generate 4γ couplings by tree-level exchange as $\zeta_i = (f_S\,m)^{-2}\,d_{i,s}$, where

$$d_{1,s} = \begin{cases} \frac{1}{2} & s = 0^+ \\ -4 & s = 0^- \\ -\frac{1}{8} & s = 2 \end{cases}, \quad d_{2,s} = \begin{cases} 0 & s = 0^+ \\ 8 & s = 0^- \\ \frac{1}{2} & s = 2 \end{cases}. \tag{8.2}$$

JHEP02(2015)165

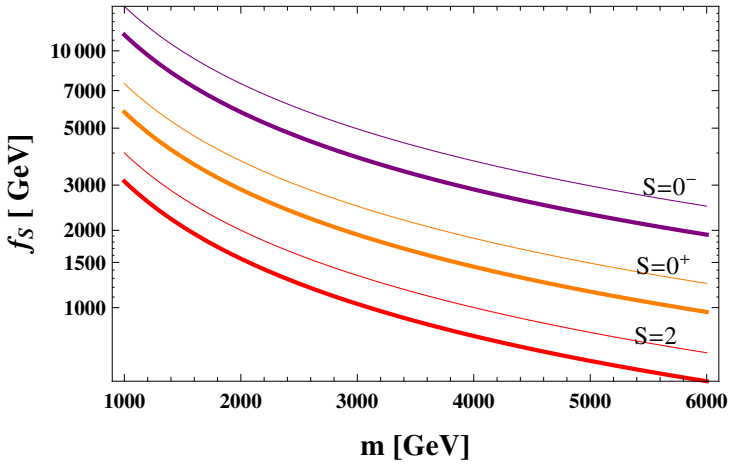

Figure 10. Sensitivities for the neutral simplified models in the (m, f_S) plane. Thick lines correspond to $5\,\sigma$, thin lines correspond to 95% CL limits. The limits are given for the medium luminosity LHC with all photons (no conversion required) and no form-factor (see table 3).

We show in figure 10 our model independent sensitivities for these three cases.

Various contributions from New Physics states are shown together with the discovery reach estimated in this paper in figure 11. We stress that this plot is valid only in the decoupling limit, so that the results based on full amplitudes presented in section 7 are not included in the plot.

Let us review the other known new physics candidates for completeness (see [3, 4] for complementary information).

- *Kaluza-Klein gravitons:* Kaluza Klein gravitons of warped extra dimensions also produce effective four-photon vertices. The contribution of the entire tower of resonances, in the case that the SM resides on the Infrared brane, leads to [3]

$$\zeta_1 = -\frac{\kappa^2}{64\tilde{k}^4}\,, \qquad \zeta_2 = \frac{\kappa^2}{4\tilde{k}^4} \tag{8.3}$$

  where $\tilde{k}$ is related to the extra dimensional curvature and sets the mass of the KK resonances as $m_{\rm KK} \approx 3.8\tilde{k}$. The quantity κ sets the coupling strength and can be taken of order unity. For $\kappa = 2$, and using the $5\,\sigma$ and 95% CL sensitivities for the medium luminosity LHC with all γs and no form-factor (see table 3), the effect of the KK resonances can be detected up to mass

$$m_{\rm KK} < 5670\,{\rm GeV}\,(5\,\sigma)\,, \quad m_{\rm KK} < 6450\,{\rm GeV}\ (95\%{\rm CL})\,. \tag{8.4}$$

  These sensitivities are competitive with respect to searches for direct production of KK resonances at the LHC.

- *Strongly-interacting dilaton:* Extensions of the Standard Model sometimes feature a new strongly-interacting sector. Provided that this sector is conformal in the UV, it is most likely explicitly broken in the IR, at least by the appearance of electroweak

JHEP02(2015)165

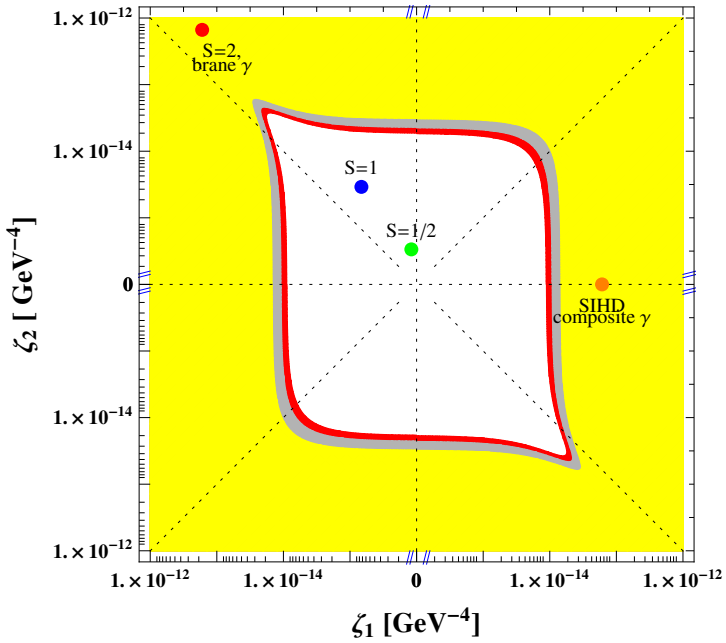

Figure 11. Experimental sensitivity and models in the (ζ_1, ζ_2) plane. Axes follow a logarithmic scale spanning $|\zeta_i| \in [10^{-12}, 10^{-16}]$. The yellow, grey, and red regions can be probed at $5\,\sigma$, $3\,\sigma$ and 95% CL using proton tagging at the LHC, while the white region remains inaccessible. The limits are given for the medium luminosity LHC with all photons (no conversion required) and no form-factor (see table 3). Also shown are contributions from electric particles with spin 1/2 and 1, charge $Q_{\rm eff} = 3$, mass $m = 1\,\text{TeV}$, the contribution from warped KK gravitons with mass $m_{\rm KK} = 3\,\text{TeV}$, $\kappa = 2$ and brane-localized photon, and the contribution from a strongly-interacting heavy dilaton (SIHD) with mass $m_\varphi = 3\,\text{TeV}$ coupled to a composite photon.

scale and QCD confinement. As a result, the spectrum of the strong sector features a neutral scalar, the so-called dilaton, whose mass lies close to the scale of conformal breaking. In the absence of fine-tuning the dilaton's couplings are unsuppressed with respect to this scale. To distinguish it from the weakly coupled (fine-tuned) light dilaton often considered in the literature we will refer to it as the Strongly-Interacting Heavy Dilaton (SIHD). If the photon is at least partially composite, it also couples strongly to the dilaton. For a pure composite photon, one gets

$$\zeta_1 = \frac{\pi^2}{2m_\varphi^4}\,, \qquad \zeta_2 = 0\,. \tag{8.5}$$

By the AdS/CFT correspondence, the SIHD is equivalent to the radion in warped extradimension scenarios where the metric presents sizeable departure from AdS_5 in the IR. The photon can couple strongly if it is either localized on the IR brane or if it has a sizable IR brane kinetic term. Using the $5\,\sigma$ and 95% CL sensitivities for the medium luminosity LHC with all γs and no form-factor (see table 3), the effect of the SIHD can be detected up to mass

$$m_\varphi < 4260\,\text{GeV}\,(5\,\sigma)\,, \quad m_\varphi < 4840\,\text{GeV}\,(95\%\text{CL})\,. \tag{8.6}$$

JHEP02(2015)165

One should notice that the expected observation of four-photon interactions at the LHC discussed in this work does not provide information on ζ_1, ζ_2 separately, nor their sign, but only on the combination eq. (7.1). In principle, more refined observables could provide information lifting this degeneracy. This would in turn provide a way of identifying various contributions. As the various amplitudes depend on different combinations of ζ_1 and ζ_2, polarization-based observables could play this role. One can notice, for example, that $\mathcal{M}_{++--}$ is exactly zero for a spin-2 particle as the KK graviton. However, in the measurement proposed in this paper, we find that no information discriminating between ζ_1, ζ_2 can be obtained by looking at the photon angular distributions.

9 Conclusion

The scheduled installation of forward proton detectors at the LHC will provide a — somewhat surprising — opportunity to measure the scattering of light-by-light, providing a new window on physics beyond the Standard Model. This paper is dedicated to the estimation of the discovery potential for light-by-light scattering at the 14 TeV LHC, especially in the case of generic new electrically charged particle of spins 1/2 and 1.

Light enough charged particles could in principle be directly produced and observed at the LHC. However such processes are highly model-dependent, and a dedicated analysis has to be set up for each specific case. In contrast, light-by-light scattering provides model-independent limits from a single precision measurement, such that both approaches are complementary.

A former estimation of the LHC sensitivity to heavy charged particles has been performed in [4] in the decoupling limit. The case of light masses i.e. lower than a few TeV, which is potentially the most interesting, is not covered in this approach, as it requires the use of ad-hoc form-factors. To avoid the introduction of such arbitrariness, we implemented the full one-loop amplitudes for spin 1/2 and spin 1, such that our simulations are valid for any mass.

The crucial feature of the forward proton detectors is that they give access to the complete kinematics of the events. This can be used to reject most of the background. The implementation of the generic one-loop amplitudes contributions — including all limiting regimes — is done in FPMC. The implementation of the full amplitudes is also useful to simulate the SM QED background. It appears that the W-loop dominates over fermion loops, and takes a simple form in the high-energy regime.

We provide the sensitivity to charged particles in the (Q_{eff}, m) plane for medium and high luminosity scenarios. For $Q_{\text{eff}} = 4$, we find that a new vector (fermion) can be detected at $5\,\sigma$ up to mass $m = 700\,\text{GeV}$ (370 GeV) and $m = 740\,\text{GeV}$ (410 GeV) respectively for the medium and high luminosity LHC configuration. The transition between EFT and full amplitudes results is also discussed quantitatively.

We also point out that new charged particles contribute to the muon anomalous gyromagnetic moment at two and three-loop. An estimate of these contributions shows that, in spite of the impressive precision of the muon g-2 measurement, it cannot compete with the LHC search we propose.

JHEP02(2015)165

The inclusive tri-photon cross section is also sensitive to the anomalous four-photon couplings since it can be produced by annihilation of a quark-antiquark pair into a photon which then splits into three photons. This channel will be studied in detail at the LHC, but we expect its sensitivity not to be as good as the reach obtained in this paper. Indeed, three photons are produced in the final state so the transverse momentum of the third photon is smaller, leading to a more complicated analysis.

The light-by-light scattering sensitivity to neutral particles in the EFT limit is also considered through simplified models. We find that warped KK gravitons and the strongly-interacting heavy dilaton can be discovered in the multi-TeV range.

Finally, looking at the $s = 0, 1/2, 1$ charged particles contributions (eq. (3.8), (3.9)), we notice that the contributions from charged loops appear to grow quite fast with the spin of the particle. If this behaviour remains true for larger spin, light-by-light scattering might constitute an interesting probe for the presence of higher-spin particles, like string excitations or strongly-interacting bound states. Further tools are however necessary to handle quantum computations involving higher-spin particles and are under developments [36].

Acknowledgments

We would like to thank O. Kepka and O. Lebedev for valuable discussions. SF acknowledges the Brazilian Ministry of Science, Technology and Innovation for financial support, and the Institute of Theoretical Physics of Sao Paulo (ICTP/SAIFR) for hospitality. GG would like to thank the Fundação de Amparo à Pesquisa do Estado de São Paulo (FAPESP) for financial support.

A The full one-loop amplitudes

In this appendix we collect for completeness the expressions for the on-shell four-photon amplitudes generated from heavy spin-1/2 and spin-1 states [6, 28]. We also compute various kinematical limits. These expressions can be applied to both SM particles (quarks, leptons, W-bosons, as well as any New Physics particles of spin $\frac{1}{2}$ and 1. In particular, for the SM contributions, we need to sum over the quark and lepton spectrum with the correct electric charges (-1 for leptons, $\frac{2}{3}$ for up type quarks, $-\frac{1}{3}$ for down-type quarks and 1 for the W-boson).

A.1 Loop functions

The loop-integrals can be expressed in terms of the functions $B(z)$, $T(z)$ and $I(z, w)$, defined as

$$\begin{aligned} \mathrm{Re}\, B(z) &= -1 + \mathrm{Re}\left[\frac{b(z)}{2}\log\left(\frac{b(z)+1}{b(z)-1}\right)\right] \\ \mathrm{Im}\, B(z) &= -\frac{\pi}{2}b(z) \qquad \text{for } z > 1\,. \end{aligned} \tag{A.1}$$

where $b(z) = \sqrt{1-1/z}$ as well as

$$\begin{aligned}\mathrm{Re}\, T(z) &= \mathrm{Re}\left[\frac{1}{4}\log^2\left(\frac{b(z)+1}{b(z)-1}\right)\right]\\ \mathrm{Im}\, T(z) &= -\pi\,\mathrm{arcosh}\,\sqrt{z} \qquad \text{for } z>1\,.\end{aligned} \tag{A.2}$$

and

$$\begin{aligned}\mathrm{Re}\, I(z,w) &= \frac{1}{2a}\,\mathrm{Re}\left[-\mathrm{Li}_2\left(\frac{a+1}{a+b(z)}\right)+\mathrm{Li}_2\left(\frac{a-1}{a+b(z)}\right)-\mathrm{Li}_2\left(\frac{a+1}{a-b(z)}\right)\right.\\ &\qquad +\mathrm{Li}_2\left(\frac{a-1}{a-b(z)}\right)-\mathrm{Li}_2\left(\frac{a+1}{a+b(w)}\right)+\mathrm{Li}_2\left(\frac{a-1}{a+b(w)}\right)\\ &\qquad \left.-\mathrm{Li}_2\left(\frac{a+1}{a-b(w)}\right)+\mathrm{Li}_2\left(\frac{a-1}{a-b(w)}\right)\right]\\ \mathrm{Im}\, I(z,w) &= \frac{\pi}{2a}\left[\Theta(z-1)\log\left(\frac{a-b(z)}{a+b(z)}\right)+\Theta(w-1)\log\left(\frac{a-b(w)}{a+b(w)}\right)\right]\,,\end{aligned} \tag{A.3}$$

where $a(z,w) = \sqrt{1-1/z-1/w}$, $\mathrm{Li}_2(z) = -\int_0^z \log(1-t)/t$ is the dilogarithm function, and $\Theta(x)$ is the units step function that is 0 (1) for $x<0$ ($x>0$).

A.2 Amplitudes

It proves useful to define the rescaled Mandelstam variables

$$s' = \frac{s}{4m^2}, \qquad t' = \frac{t}{4m^2} \qquad u' = \frac{u}{4m^2} \tag{A.4}$$

where $s'+t'+u' = 0$, and $-s' \le t, u \le 0$. Here, m denotes the mass of the particle in the loop. The helicity amplitudes for fermion loops have been computed in ref. [28], they are given as

$$\begin{aligned}\mathcal{M}^f_{++++} &= 1+2\left[\frac{t'-u'}{s'}\right]\left[B(t')-B(u')\right]+\left[\frac{2(t'^2+u'^2)}{s'^2}-\frac{2}{s'}\right]\left[T(t')+T(u')\right]\\ &\quad+\left[\frac{1}{2s't'}-\frac{1}{t'}\right]I(s',t')+\left[\frac{1}{2s'u'}-\frac{1}{u'}\right]I(s',u')\\ &\quad+\left[\frac{4}{s'}+\frac{1}{t'}+\frac{1}{u'}+\frac{1}{2t'u'}-\frac{2(t'^2+u'^2)}{s'^2}\right]I(t',u')\\ \mathcal{M}^f_{+++-} &= -1-\left[\frac{1}{s'}+\frac{1}{t'}+\frac{1}{u'}\right]\left[T(s')+T(t')+T(u')\right]\\ &\quad+\left[\frac{1}{u'}+\frac{1}{2s't'}\right]I(s',t')+\left[\frac{1}{t'}+\frac{1}{2s'u'}\right]I(s',u')+\left[\frac{1}{s'}+\frac{1}{2t'u'}\right]I(t',u')\\ \mathcal{M}^f_{++--} &= -1+\frac{1}{2s't'}I(s',t')+\frac{1}{2s'u'}I(s',u')+\frac{1}{2t'u'}I(t',u')\end{aligned} \tag{A.5}$$

The helicity amplitudes for vector loops taken from [6] read

$$\begin{aligned}\mathcal{M}^v_{++++} &= -\frac{3}{2}-3\left[\frac{t'-u'}{s'}\right]\left[B(t')-B(u')\right]\\ &\quad-\frac{1}{s'}\left[8s'-3-6\frac{t'u'}{s'}\right]\left[T(t')+T(u')-I(t',u')\right]\\ &\quad-\frac{3}{s'}I(t',u')-4\left(s'-\frac{1}{4}\right)\left(s'-\frac{3}{4}\right)\left[I(s',t')\frac{1}{s't'}+I(s',u')\frac{1}{s'u'}+I(t',u')\frac{1}{t'u'}\right]\end{aligned} \tag{A.6}$$

whereas the other two are simply rescaled w.r.t. the fermion result, $\mathcal{M}^v_{+++-} = -\frac{3}{2}M^f_{+++-}$ and $\mathcal{M}^v_{++--} = -\frac{3}{2}M^f_{++--}$.

B Limits

B.1 Low-energy approximation

In the low-energy limit $s', |t'|, |u'| \ll 1$ the amplitudes become

$$\mathcal{M}^f_{++++} = -\frac{22}{45}s'^2\,, \qquad \mathcal{M}^f_{++--} = \frac{2}{15}(s'^2+t'^2+u'^2)\,, \qquad \mathcal{M}^f_{+++-} = \mathcal{O}(s'^3)\,. \tag{B.1}$$

for the fermion loops and

$$\mathcal{M}^v_{++++} = -\frac{28}{5}s'^2\,, \qquad \mathcal{M}^v_{+++-} = \frac{1}{5}(s'^2+t'^2+u'^2)\,, \qquad \mathcal{M}^v_{++--} = \mathcal{O}(s'^3)\,. \tag{B.2}$$

for the vector loops.

B.2 High-energy approximation

In the high-energy limit $s', |t'|, |u'| \gg 1$, at fixed scattering angle, the fermion-loop induced amplitudes go to constants

$$\begin{aligned}\mathcal{M}^f_{++++} &= 1 - \frac{(t'-u')}{s'}\left[\ell(t')-\ell(u')\right] + \frac{t'^2+u'^2}{2s'^2}\left([\ell(t')-\ell(u')]^2+\pi^2\right)+\dots \\ \mathcal{M}^f_{+++-} &= \mathcal{M}^f_{++--} = -1+\dots\end{aligned} \tag{B.3}$$

with the remaining amplitudes given by eq. (3.11) and we have defined the shorthand $\ell(z) \equiv \log(-1/4z) = -\log(-4z-i\epsilon)$. The vector-loop induced amplitudes on the other hand show a logarithmic divergence [6, 45].

$$\begin{aligned}\mathcal{M}^v_{++++} &= -\frac{3}{2} + \frac{3}{2}\frac{(t'-u')}{s'}[\ell(t')-\ell(u')] - 2\left(1-\frac{3}{4}\frac{t'u'}{s'^2}\right)\left([\ell(t')-\ell(u')]^2+\pi^2\right) \\ &\quad -2s'^2\left(\frac{1}{s't'}\ell(s')\ell(t') + \frac{1}{s'u'}\ell(s')\ell(u') + \frac{1}{t'u'}\ell(t')\ell(u')\right)\end{aligned} \tag{B.4}$$

$$\mathcal{M}^v_{+++-} = \mathcal{M}^v_{++--} = \frac{3}{2}+\dots \tag{B.5}$$

This has the important consequence that at LHC energies, the W-loop is dominating the loops of all the SM fermions (including the top).

B.3 Forward and backward limits

For fermions, the forward limit ($|t'| \ll s'$) has also been computed in ref. [28]:

$$\begin{aligned}\mathcal{M}^f_{++++} &= 1 + \left(2-\frac{1}{s'}\right)B(s') + \left(-4+\frac{1}{s'}\right)B(-s') + \left(\frac{1}{s'}-\frac{1}{2s'^2}\right)T(s') \\ &\quad + \left(2-\frac{1}{s'}-\frac{1}{2s'^2}\right)T'(-s')\,, \\ \mathcal{M}^f_{++--} &= -1 - \frac{1}{s'}B(s') + \frac{1}{s'}B(-s') - \frac{1}{2s'^2}T(s') - \frac{1}{2s'^2}T(-s')\,,\end{aligned} \tag{B.6}$$

JHEP02(2015)165

as well as $\mathcal{M}^f_{+-+-}(s') = M^f_{++++}(-s')$ and $M^f_{+--+} = M^f_{+++-} = 0$. Similarly, in the spin-1 case, we obtain

$$\mathcal{M}^v_{++++} = -\frac{3}{2} + \frac{8}{s'}\left(s' - \frac{1}{4}\right)\left(s' - \frac{3}{4}\right)\left(B(s') - B(-s') + \frac{1}{2s'}T(s') + \frac{1}{2s'}T(-s')\right) + 3B(-s') + \left(\frac{3}{s'} - 8\right)T(-s')\,, \tag{B.7}$$

while $M^v_{++--} = -\frac{3}{2}M^f_{++--}$, $\mathcal{M}^v_{+-+-}(s') = M^v_{++++}(-s')$, and $M^v_{+--+} = M^v_{+++-} = 0$. The backward limit ($|u'| \ll s'$) is obtained by the interchange $M_{+-+-} \leftrightarrow M_{+--+}$. Notice that the forward/backward and high energy limits do not commute.

C Expressions for the amplitudes in EFT

Starting from the effective Lagrangian,

$$\mathcal{L}_{\text{eff}} = \zeta_1\ (F_{\mu\nu}F^{\mu\nu})^2 + \zeta_2\ F_{\mu\nu}F^{\nu\rho}F_{\rho\lambda}F^{\lambda\mu} \tag{C.1}$$

one can compute

$$\begin{aligned}
\alpha^2_{em}\mathcal{M}_{++++} &= -\frac{1}{4}\,(4\zeta_1 + 3\zeta_2)\,s^2 \\
\alpha^2_{em}\mathcal{M}_{++--} &= -\frac{1}{4}\,(4\zeta_1 + \zeta_2)\,(s^2 + t^2 + u^2) \\
\alpha^2_{em}\mathcal{M}_{+++-} &= \mathcal{O}(s'^3)\,.
\end{aligned} \tag{C.2}$$

In case the ζ_i arise in the low-energy limit of fermion and gauge loops eq. (3.9) these expressions precisely reproduce the low-energy limit of the amplitudes given in eqs. (B.1) and (B.2).

References

[1] K. Agashe, R. Contino and A. Pomarol, *The minimal composite Higgs model*, *Nucl. Phys.* **B 719** (2005) 165 [hep-ph/0412089] [INSPIRE].

[2] K. Agashe, A. Delgado, M.J. May and R. Sundrum, *RS1, custodial isospin and precision tests*, *JHEP* **08** (2003) 050 [hep-ph/0308036] [INSPIRE].

[3] S. Fichet and G. von Gersdorff, *Anomalous gauge couplings from composite Higgs and warped extra dimensions*, *JHEP* **03** (2014) 102 [arXiv:1311.6815] [INSPIRE].

[4] S. Fichet et al., *Probing new physics in diphoton production with proton tagging at the Large Hadron Collider*, *Phys. Rev.* **D 89** (2014) 114004 [arXiv:1312.5153] [INSPIRE].

[5] M. Boonekamp et al., *FPMC: a generator for forward physics*, arXiv:1102.2531 [INSPIRE].

JHEP02(2015)165

[6] G. Jikia and A. Tkabladze, *Photon-photon scattering at the photon linear collider*, *Phys. Lett.* **B 323** (1994) 453 [hep-ph/9312228] [INSPIRE].

[7] ATLAS collaboration *Letter of Intent for the Phase-I Upgrade of the ATLAS Experiment*, CERN-LHCC-2011-012 (2011).

[8] CMS and TOTEM collaboration, *CMS-TOTEM precision proton spectrometer*, CERN-LHCC-2014-021 (2014).

[9] E. Chapon, C. Royon and O. Kepka, *Anomalous quartic $WW\gamma\gamma$, $ZZ\gamma\gamma$ and trilinear $WW\gamma$ couplings in two-photon processes at high luminosity at the LHC*, *Phys. Rev.* **D 81** (2010) 074003 [arXiv:0912.5161] [INSPIRE].

[10] O. Kepka and C. Royon, *Anomalous $WW\gamma$ coupling in photon-induced processes using forward detectors at the LHC*, *Phys. Rev.* **D 78** (2008) 073005 [arXiv:0808.0322] [INSPIRE].

[11] I. Sahin and S.C. Inan, *Probe of unparticles at the LHC in exclusive two lepton and two photon production via photon-photon fusion*, *JHEP* **09** (2009) 069 [arXiv:0907.3290] [INSPIRE].

[12] S. Atag, S.C. Inan and I. Sahin, *Extra dimensions in $\gamma\gamma \to \gamma\gamma$ process at the CERN-LHC*, *JHEP* **09** (2010) 042 [arXiv:1005.4792] [INSPIRE].

[13] R.S. Gupta, *Probing quartic neutral gauge boson couplings using diffractive photon fusion at the LHC*, *Phys. Rev.* **D 85** (2012) 014006 [arXiv:1111.3354] [INSPIRE].

[14] P. Lebiedowicz, R. Pasechnik and A. Szczurek, *Search for technipions in exclusive production of diphotons with large invariant masses at the LHC*, *Nucl. Phys.* **B 881** (2014) 288 [arXiv:1309.7300] [INSPIRE].

[15] H. Sun, *Probe anomalous $tq\gamma$ couplings through single top photoproduction at the LHC*, *Nucl. Phys.* **B 886** (2014) 691 [arXiv:1402.1817] [INSPIRE].

[16] H. Sun, *Large extra dimension effects through light-by-light scattering at the CERN LHC*, *Eur. Phys. J.* **C 74** (2014) 2977 [arXiv:1406.3897] [INSPIRE].

[17] H. Sun, *Dark matter searches in jet plus missing energy events in γp collisions at the CERN LHC*, *Phys. Rev.* **D 90** (2014) 035018 [arXiv:1407.5356] [INSPIRE].

[18] I. Sahin et al., *Graviton production through photon-quark scattering at the LHC*, arXiv:1409.1796 [INSPIRE].

[19] S.C. Inan, *Dimension-six anomalous $tq\gamma$ couplings in $\gamma\gamma$ collision at the LHC*, arXiv:1410.3609 [INSPIRE].

[20] D. d'Enterria and G.G. da Silveira, *Observing light-by-light scattering at the Large Hadron Collider*, *Phys. Rev. Lett.* **111** (2013) 080405 [arXiv:1305.7142] [INSPIRE].

[21] H. Terazawa, *Two photon processes for particle production at high-energies*, *Rev. Mod. Phys.* **45** (1973) 615 [INSPIRE].

[22] V.M. Budnev, I.F. Ginzburg, G.V. Meledin and V.G. Serbo, *The two photon particle production mechanism. Physical problems. Applications. Equivalent photon approximation*, *Phys. Rept.* **15** (1975) 181 [INSPIRE].

[23] V.A. Khoze, A.D. Martin and M.G. Ryskin, *Prospects for new physics observations in diffractive processes at the LHC and Tevatron*, *Eur. Phys. J.* **C 23** (2002) 311 [hep-ph/0111078] [INSPIRE].

[24] E. Gotsman, E. Levin, U. Maor, E. Naftali and A. Prygarin, *Survival probability of large rapidity gaps*, hep-ph/0511060 [INSPIRE].

JHEP02(2015)165

[25] M. Dyndal and L. Schoeffel, *The role of finite-size effects on the spectrum of equivalent photons in proton-proton collisions at the LHC*, *Phys. Lett.* **B 741** (2015) 66 [arXiv:1410.2983] [INSPIRE].

[26] R. Karplus and M. Neuman, *Non-linear interactions between electromagnetic fields*, *Phys. Rev.* **80** (1950) 380 [INSPIRE].

[27] R. Karplus and M. Neuman, *The scattering of light by light*, *Phys. Rev.* **83** (1951) 776 [INSPIRE].

[28] V. Costantini, B. De Tollis and G. Pistoni, *Nonlinear effects in quantum electrodynamics*, *Nuovo Cim.* **A 2** (1971) 733 [INSPIRE].

[29] C. Royon, *Forward Physcis at the LHC*, presentation at the *Open LHCC meeting*, September 24–25, CERN, Geneva (2014).

[30] CDF collaboration, T. Aaltonen et al., *Search for exclusive $\gamma\gamma$ production in hadron-hadron collisions*, *Phys. Rev. Lett.* **99** (2007) 242002 [arXiv:0707.2374] [INSPIRE].

[31] S. Fichet, G. Gersdorff, V. Goncalvez, M. Rangel and C. Royon, *Search for $\gamma\gamma\gamma\gamma$ quartic anomalous couplings in the heavy ion mode at the LHC*, in preparation.

[32] D. Barducci et al., *Framework for model independent analyses of multiple extra quark scenarios*, *JHEP* **12** (2014) 080 [arXiv:1405.0737] [INSPIRE].

[33] PARTICLE DATA GROUP collaboration, K. Olive et al., *Review of particle physics*, *Chin. Phys.* **C 38** (2014) 090001 [INSPIRE].

[34] W. Heisenberg and H. Euler, *Consequences of Dirac's theory of positrons*, *Z. Phys.* **98** (1936) 714 [physics/0605038] [INSPIRE].

[35] L.A. Anchordoqui et al., *String resonances at hadron colliders*, *Phys. Rev.* **D 90** (2014) 066013 [arXiv:1407.8120] [INSPIRE].

[36] S. Fichet and G. Gersdorff, in preparation.

[37] Z. Bern, A. De Freitas, L.J. Dixon, A. Ghinculov and H.L. Wong, *QCD and QED corrections to light by light scattering*, *JHEP* **11** (2001) 031 [hep-ph/0109079] [INSPIRE].

[38] N. Cartiglia and C. Royon, *The AFP and CT-PPS projects*, *Int. J. Mod. Phys.* **A 29** (2014) 1446017 [INSPIRE].

[39] G. Corcella et al., *HERWIG 6.5 release note*, hep-ph/0210213 [INSPIRE].

[40] J. Monk and A. Pilkington, *ExHuME: a Monte Carlo event generator for exclusive diffraction*, *Comput. Phys. Commun.* **175** (2006) 232 [hep-ph/0502077] [INSPIRE].

[41] C. Royon, L. Schoeffel, S. Sapeta, R.B. Peschanski and E. Sauvan, *A global analysis of inclusive diffractive cross sections at HERA*, *Nucl. Phys.* **B 781** (2007) 1 [hep-ph/0609291] [INSPIRE].

[42] ATLAS collaboration, *Performance assumptions based on full simulation for an upgraded ATLAS detector at a High-Luminosity LHC*, ATL-PHYS-PUB-2013-009 (2013).

[43] A. Pukhov et al., *CompHEP: a package for evaluation of Feynman diagrams and integration over multiparticle phase space*, hep-ph/9908288 [INSPIRE].

[44] COMPHEP collaboration, E. Boos et al., *CompHEP 4.4: automatic computations from Lagrangians to events*, *Nucl. Instrum. Meth.* **A 534** (2004) 250 [hep-ph/0403113] [INSPIRE].

[45] G.J. Gounaris, P.I. Porfyriadis and F.M. Renard, *The $\gamma\gamma \to \gamma\gamma$ process in the standard and SUSY models at high-energies*, *Eur. Phys. J.* **C 9** (1999) 673 [hep-ph/9902230] [INSPIRE].

JHEP02(2015)165